Boreal-winter teleconnections with tropical Indo-Pacific rainfall in HighResMIP historical simulations from the PRIMAVERA project

Franco Molteni [1], Christopher D. Roberts [1], Retish Senan [1], Sarah P. E. Keeley [1], Alessio Bellucci [2], Susanna Corti [3], Ramon Fuentes Franco [4], Rein Haarsma [5], Xavier Levine [6], Dian Putrasahan [7], Malcolm J. Roberts [8] and Laurent Terray [9]

1. *European Centre for Medium-Range Weather Forecasts (ECMWF), Reading, United Kingdom*
2. *Fondazione Centro Euro-Mediterraneo sui Cambiamenti Climatici (CMCC), Bologna, Italy*
3. *Institute of Atmospheric Sciences and Climate, ISAC-CNR, Bologna, Italy*
4. *Swedish Meteorological and Hydrological Institute (SMHI), Norrköping, Sweden*
5. *Royal Netherlands Meteorological Institute (KNMI), De Bilt, The Netherlands*
6. *Barcelona Supercomputing Center - Centro Nacional de Supercomputación (BSC-CNS), Barcelona, Spain*
7. *Max-Planck-Institut für Meteorologie, (MPI-M), Hamburg, Germany*
8. *Met Office Hadley Centre, Exeter, United Kingdom*
9. *Climat, Environnement, Couplages, Incertitudes, CECI, Université de Toulouse, CNRS, CERFACS, Toulouse, France*

Climate Dynamics

Supplementary material

Corresponding author:

Franco Molteni, ECMWF, Reading RG2 9AX, United Kingdom

Email: franco.molteni@ecmwf.int

ORCID id.: 0000-0003-0651-4566

S1. Sampling properties of NAO indices in teleconnection patterns, and their inter-decadal variability.

In Sections 2 and 3, we noticed that although both the WCIO and NINO4 teleconnections have a NAO component, the response over the Atlantic does not project onto the same pattern. Consequently, different NAO indices (see Eqs. 3a and 3b) may be better suited to represent the North Atlantic response to different sources and in different periods. In Fig. 5b, we presented estimates of probability functions (PDFs) of an Atlantic-wide NAO index (Eq. 3a) from re-sampled datasets, noting that our estimates were appropriate for estimating uncertainties in simulations which spanned the full 1950-2010 period.

In this Supplement, we wish to extend this discussion in two ways:

a) we compare PDFs for both the Atlantic-wide (Eq. 3a) and the Portugal-Iceland centred index (Eq. 3b);

b) we examine how these indices change if we compute teleconnections from samples that span either the first or the second half of the period.

Point (a) is addressed in Fig. S1, where PDFs for the two NAO indices computed from WCIO and NINO4 teleconnections are compared. For the two teleconnection patterns that have a positive NAO component (WCIO in DJ and NINO4 in ND), using the Portugal-Iceland index results in a further shift of the PDF towards positive values. However, for both indices the sign of the response is consistently positive. A much larger difference is noticed for the NINO4 response in late-winter, which has a consistent negative sign only when the Atlantic-wide index (Eq. 3a) is used.

With regard to point (b), teleconnections computed from the 1981-2010 period (the second half of our 60-year sample) have been presented in Fig. 4. Here, in Fig. S2 we show the same teleconnections computed from CERA20C in the first part of the record, 1951-1980 (to be compared with the left-hand column of Fig. 4). For these calculations (as well as for Fig. 4), anomalies are computed with respect to the appropriate 30-year mean. At first glance, the 1951-1980 patterns appear to differ from those in the full record (Fig. 3) more than those from the 1981-2010 period, especially so for the WCIO teleconnection and the NINO4 teleconnection in early winter. However, when looking at the Atlantic signal, one finds that a NAO-like dipolar response is still present, but has been shifted to the south.

It should be remembered that the full-record patterns shown in Fig. 3 are not simply the average of the patterns computed in the two sub-samples, because (as clearly shown in Sect. 5) the mean NH circulation in the two 30-year periods is substantially different. In the 60-year sample, anomalies are computed with respect to the 60-year mean, and therefore the inter-decadal variability of both tropical rainfall and NH geopotential height contribute to the teleconnections shown in Fig. 3.

The values of the two NAO indices defined by Eq. 3a and 3b in the 3 teleconnection patterns and the two separate 30-year periods are listed in Table S1. In the last row of the table, we also show the values of the Portugal-Iceland index if the latitudes of the two boxes used in Eq. 3b are shifted 5 degrees to the south (in this case, Portugal and Iceland are located at the northern edge of the boxes instead of being at the centre). These values confirm that:

- the negative NAO response to NINO4 rainfall is best described by the Atlantic-wide index, and its change from the 1951-1980 to the 1981-2010 period is relatively small;
- the Portugal-Iceland index changes markedly between the two 30-year periods, but the change is substantially reduced if one recomputes the index with a 5^{o} southward shift.

The difference in NH mean flow between the two periods also projects strongly on the NAO, implying a shift towards a stronger Atlantic jet with a more northerly position in the latter period (Fig. 13b). Therefore it is appropriate to say that, when the WCIO and early-winter NINO4 teleconnections are computed with respect the mean of each period, the Atlantic response show a dipolar structure which shifts in latitude following the location of the jet maximum.

	WCIO DJ 1950-1979	**NINO4 ND** 1950-1979	**NINO4 JF** 1951-1980	**WCIO DJ** 1980-2009	**NINO4 ND** 1980-2009	**NINO4 JF** 1981-2010
NAO 70W-20W	6.8	12.3	-34.4	40.4	24.4	-35.7
NAO Portugal-Iceland	8.8	13.5	-8.8	51.6	31.5	-17.9
NAO Por-Icl, shifted 5^{o} south	16.6	26.6	-8.0	37.1	34.5	-9.3

Table S1 Values of different NAO indices (see Eqs. 3a, 3b) in teleconnection patterns computed in the first and second half of the 60-year CERA20C record (1950/51 to 1979/80 and 1980/81 to 2009/10 respectively). All anomalies are computed with respect to the appropriate 30-year mean.

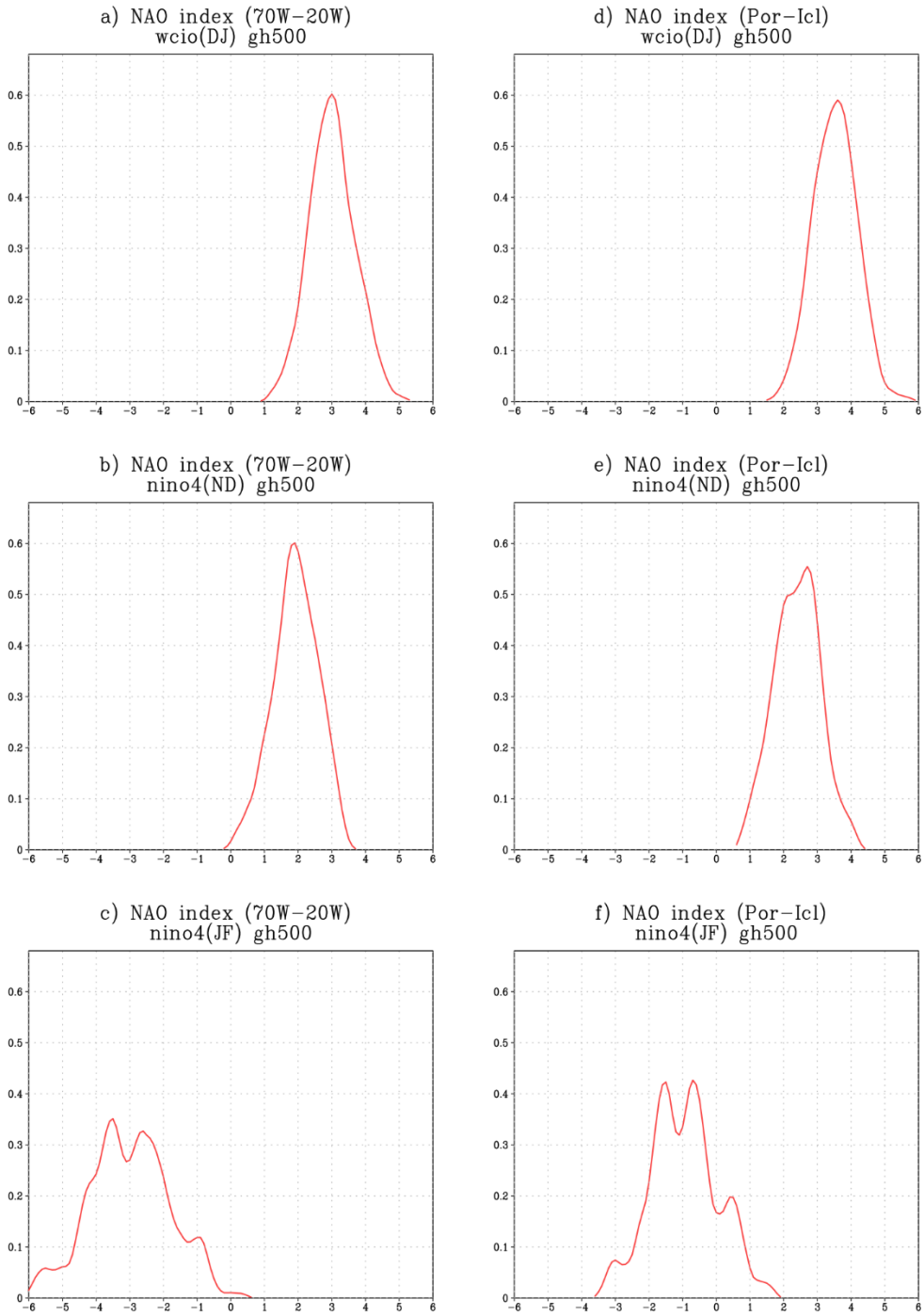

Fig. S1 Probability density function of the NAO indices (in dam) from Eq. 3a (left) and Eq. 3b (right) in the NH teleconnection patterns with tropical rainfall in WCIO (top), NINO4 in ND (centre), NINO4 in JF (bottom).

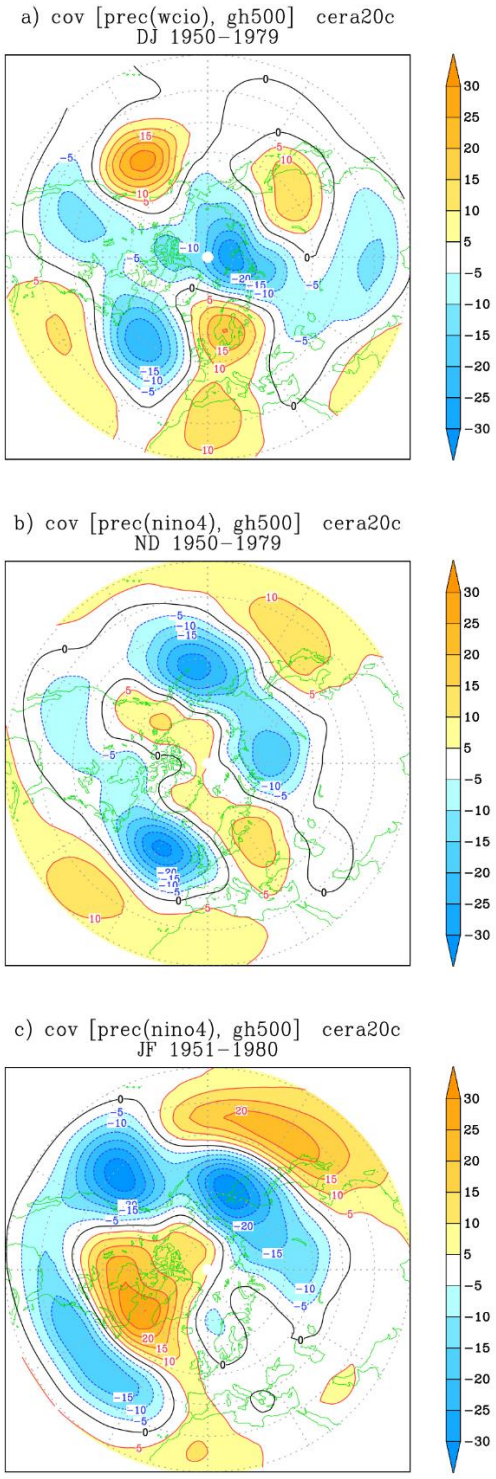

Fig. S2 a) covariance of NH 500-hPa height with WCIO rainfall in DJ; b) covariance with NINO4 rainfall in ND; c) covariance with NINO4 rainfall in JF. Data from CERA20C in winters 1950/51 to 1979/80.

S2. Discussion on the differences between WCIO teleconnections in the ECMWF uncoupled and coupled high-resolution ensembles.

In Section 4.1 of the main paper, it was noted that the NH teleconnection with WCIO rainfall was poorly represented in the coupled high-resolution historical ensemble run with the ECMWF model, whereas the simulation from the AMIP ensembles (at both resolution) showed a stronger NAO signal (Fig. 6). It was also noted that a substantial variability was found in the WCIO teleconnection patterns from different coupled ensemble members (Fig. 8), with the first two members showing a particularly poor performance. Here, we provide additional diagnostics aimed at answering two related questions:

1) What aspects of the differences in mean state and variability between the uncoupled and coupled ensembles may be responsible for the degradation of the WCIO teleconnection in the coupled ensemble?
2) Do the first two members of the coupled ensemble differ significantly from the other members in aspects related to coupled phenomena?

As a first step, it is appropriate to look at the bias in the two variables used to compute the teleconnections, namely tropical precipitation and N.Hem. 500-hPa height in December-January (DJ). These are shown in Fig. S3 for the high-resolution AMIP (AMIP-H), the first two members and the last four members of the high-resolution coupled historical ensemble (CHist-H). For precipitation, both the AMIP-H and the CHist-H ensemble tend to overestimate rainfall across most of the tropical Indo-Pacific domain, but the bias in CHist-H is substantially stronger. On the other hand, there are no significant differences between the biases of different members of the coupled ensemble. A notable feature in these rainfall biases is the overestimation of rainfall over the tropical western Indian Ocean; in CHist-H, the maximum bias here exceeds 5 mm/day, which is much larger than the typical amplitude of the observed interannual variability in this region (~ 1.5 mm/day).

The N.Hem. biases in 500-hPa height show a similar story, with a much smaller bias in the AMIP-H ensemble and hardly any difference between the coupled members with poor teleconnections and the other CHist-H members. It is worth noting that, consistently with the larger positive rainfall bias in the western Indian Ocean compared to AMIP-H, the 500-hPa height bias in CHist-H shows a stronger dipole pattern over the North Atlantic which has a positive NAO signature. Also, the stronger negative bias over the North Pacific in CHist-H is likely to be related to its stronger rainfall bias in the central equatorial Pacific, as in a typical ENSO teleconnection.

Can the larger bias justify the weaker WCIO teleconnection in CHist-H? Although it is likely that a change in mean state may affect the propagation of Rossby waves from the tropics to higher latitudes (see eg the recent studies of Lee at al. (2019) and Tseng et al. (2020) on subseasonal teleconnections), it should be noted that the larger North Pacific bias does not prevent CHist-H from reproducing the late-winter teleconnection from the NINO4 region with high fidelity (see Fig. 6i). However, the North Atlantic may not behave in such a linear way, especially if the NAO regime-like variability is critically dependent on the NAO wave component being close to resonance given the *observed* mean flow (Molteni and Kucharski 2019).

Looking now at variability in different ensembles, it was noted in Sect. 4.1 that the two members of CHist-H with very weak WCIO teleconnections also showed a larger ENSO variability than both re-analysis and the other four members (as measured by the standard deviation of the NINO3.4 SST; see Fig. 9b). In order to better understand how ENSO variability affects the WCIO teleconnection, it is useful to look at how rainfall variability is co-varying in different parts of the tropical Indo-Pacific

domain. In Fig. S4a and S4b, we show covariance maps of DJ rainfall across this domain with the normalised rainfall averages in the WCIO and NINO4 regions, computed from CERA20C data; figs. S4c and S4c show the corresponding maps for the AMIP-H ensemble.

In the re-analysis maps, both the WCIO and the NINO4 rainfall covariances show a tripolar pattern, with positive anomalies in the Indian Ocean west of 90E and in the central Pacific, and negative anomalies around the Maritime Continents. The main difference between the two maps is the relative strength of the two positive anomalies, which reflects the location of the "source" region. It is worth noting that the NINO4 covariance closely resembles the leading EOF of monthly Indo-Pacific rainfall shown in Fig. 1a, while the WCIO covariance is a good match for the Indian-West Pacific EOF shown in Fig. 1b. The AMIP-H ensemble simulates these patterns with very good fidelity, with a correct location of the main anomaly centres and an accurate simulation of their amplitude. Over the WCIO region (west of 90E), both the re-analysis and the AMIP-H maps show rainfall anomalies are positive both north and south of the Equator; this is likely to induce a Kelvin-wave response to the associated diabatic heating.

Fig. S5 shows the corresponding covariance patterns computed from the first two (panels a, b) and the last four members (panels c, d) of CHist-H. While over the Pacific the coupled model covariances provide a good simulation of the re-analysis patterns, over the central Indian Ocean the meridional symmetry of the rainfall anomalies is broken. In both the WCIO and NINO4 covariances from CHist-H data, rainfall anomalies of positive sign are confined north of the Equator between 70E and 90E, while negative anomalies to the south are connected to the negative centre located west of Sumatra. This is particularly evident in the NINO4 covariance, where the negative rainfall signal south of the Equator extends westward as far as 60E. Although the general pattern of these rainfall teleconnections is rather similar between the first two and the remaining ensemble members, the stronger ENSO variability in the former group is reflected in stronger amplitudes of the Pacific and eastern Indian Ocean rainfall anomalies, and an even stronger asymmetry in the central Indian Ocean.

How is the variable intensity of the ENSO signal, and the replacement of a symmetric with an anti-symmetric diabatic forcing in the central Indian Ocean going to affect the teleconnections? In Fig. S6, we compare 500-hPa height teleconnections computed from various indices of Indian Ocean rainfall using CERA20C data. As a reference, the 'standard' WCIO teleconnection shown in Fig. 3a is replicated here in Fig. S6a. Fig. S6b shows the teleconnection computed again from the WCIO region, but using only the component of the rainfall data which is linearly un-correlated with the NINO3.4 SST. Since the 'canonical' teleconnection form ENSO in mid-to-late winter shows negative height anomalies over the North Pacific and a negative NAO signal, subtracting the influence of ENSO results in a reinforcement of the NAO component and a weakening of North Pacific negative anomalies in the WCIO teleconnection. The partially compensating effect of teleconnections from the Indian and central Pacific oceans has been discussed in many earlier studies (e.g. Annamalai et al 2007; Fletcher and Cassou 2015; Molteni et al. 2015). Although this compensation means that one should expect a weaker total signal in the WCIO teleconnection in the presence of a stronger ENSO signal, the difference between Fig. S6a and S6b is not so strong to justify an almost total cancellation with an ENSO variability increase of about 20% (as in the first two members of CHist-H).

To explore the effect of the symmetry vs. asymmetry of the rainfall anomalies in the central Indian Ocean, we have defined two further indices from the rainfall anomalies between 70E and 90E. The first index (CIO-ave) is just the average anomaly between 10N and 10S, while CIO-dif is difference between the anomalies north and south of the equator (10N-0 and 0-10S respectively). The 500-hPa height teleconnections from these two indices are shown in Fig. S6c and S6d respectively. While the

teleconnection from CIO-ave is very similar (if partially weaker) to the teleconnection from the wider WCIO region, the teleconnection of a north-south rainfall dipole in the central Indian Ocean has only a marginal response over the Atlantic and Europe, while it tends to strengthen the North Pacific jet around 50N. This suggests that the replacement of a symmetric rainfall signal in AMIP-H with an anti-symmetric one in CHist-H is the main cause of the deterioration of the WCIO teleconnection in the coupled ensemble. The fact that the anti-symmetric signal is particularly evident in the NINO4 teleconnection, and therefore gets stronger with stronger ENSO amplitudes (cf. Figs S5b and S5d) also provides an explanation for the very weak teleconnections in the CHist members with larger-than-average ENSO variability.

The different behaviour of the AMIP-H and CHist-H ensembles with respect to the simulation of Indian Ocean rainfall suggests that systematic errors in the simulation of SST variability may be responsible for the anti-symmetric rainfall pattern found in CHist-H. To address this question, Table S2 lists the correlation of the CIO-dif rainfall index with SST anomalies in the NINO3.4 region and in the eastern equatorial Indian Ocean west of Sumatra (EEIO: 90E-110E, 0-10S) in both the AMIP-H and CHist-H ensembles, as well as in re-analysis. Previous investigations showed that the ECMWF coupled model used in PRIMAVERA and in the seasonal forecast SEAS5 produced a much larger SST variability than observations in the EEIO region during boreal autumn (by almost a factor of 2 in CHist-H; see again Table S2 and also Fig. 4 in Johnson et al. 2019). For this reason, in addition to contemporaneous correlation, Table S2 shows the correlation of the rainfall CIO-dif index in DJ with the EEIO SST in October-November (ON).

In the AMIP-H ensemble, where SST is prescribed from the HasISST2 dataset, the simulated correlations of the CIO-dif index do not differ substantially from the re-analysis values, all of them being of rather low amplitude. In particular, the fact that lagged correlations with autumn EEIO SST are very close to the DJ contemporaneous correlations is correctly reproduced. On the other hand, in the CHist-H ensemble the differences from re-analysis are remarkable, with the positive correlation with NINO3.4 SST being about 3 time larger, and the negative lagged correlation with ON SST west of Sumatra going from -0.22 to -0.76. It appears that the anti-symmetric rainfall signal in the central Indian Ocean is strictly controlled by the autumn SST in the eastern part of the ocean, with cold SST anomalies west of Sumatra shifting rainfall north of the Equator; such a signal persists from ON to the following winter months. In turn, such cold SST anomalies are often associated with warm anomalies in the central Pacific, and this is reflected in the positive correlation between the CIO-dif and the NINO3.4 indices.

Finally, we tested the impact of SST variability in the EEIO on the teleconnection of DJ WCIO rainfall by constructing a “merged” ensemble member from the six members of CHist-H. For each autumn-winter season in the 60-year record, we selected data from the member for in which the EEIO SST anomaly in ON was closest to the HadISST2 anomaly. Then, from the DJ data of the merged dataset, we computed the covariances of normalised WCIO rainfall with rainfall itself and with N.Hem. 500-hPa height; these fields are shown in Fig. S7a and S7b respectively.

Comparing the rainfall covariance in Fig. S7a with those of the original members of CHist-H in Fig. S5a and S5c, one can see a reduction of the negative rainfall anomaly south of the Equator between 70E and 90E, with the centre of the positive anomaly being closer to the Equator. Also, the covariance with central Pacific rainfall is reduced, since the selection process removes cases with larger-than observed EEIO SST anomaly in autumn, which in turn are often followed by strong ENSO anomalies in winter. These changes in the rainfall pattern are accompanied by a clear increase of the positive NAO signal in the 500-hPa teleconnection (Fig. S7b) with respect to the original members of CHist-H (cf. Fig. 8 in the main paper). For the “merged” member, the covariance between the

normalised WCIO index and the Portugal-Iceland NAO index reaches 30 m, larger than any of the single-member values shown in Fig. 9b, and only about 20% weaker than the observed covariance of 36 m. On the other hand, significant differences from the observed pattern are still present in the North Pacific, partly due to the reduction of the rainfall signal from the central Pacific.

In summary, although we cannot rule out other factors affecting the teleconnection from Indian Ocean rainfall, it seems that the excessive variability of autumn SST in the EEIO plays an important role in the deterioration of wintertime teleconnections to the northern extratropics, and the North Atlantic in particular, in the ECMWF coupled ensemble. Since EEIO and central Pacific SST variability are anti-correlated, the deterioration due to the (incorrect) dipolar pattern of rainfall anomalies in the central Indian Ocean is stronger in the presence of large-amplitude ENSO events; this effect (in addition to the observed partial compensation of teleconnections from the Indian Ocean and the central Pacific) explains why the CHist-H members with largest ENSO variability are also those with weakest WCIO teleconnection.

	Stand. deviation SST (EEIO, ON) [^{o}C]	Correlation Prec (CIO-dif, DJ), SST (NINO3.4, DJ)	Correlation Prec (CIO-dif, DJ), SST (EEIO, DJ)	Correlation Prec (CIO-dif, DJ), SST (EEIO, ON)
HadISST2 SST CERA20C prec.	0.36	0.14	- 0.21	- 0.22
AMIP-H	0.36	0.16	- 0.08	- 0.20
CHist-H	0.65	0.48	- 0.22	- 0.76

Table S2. Statistics on the variability and correlation of SST and rainfall indices in Indian Ocean and central Pacific regions, from observational datasets and the ECMWF high-res. AMIP and coupled historical ensembles.

References

Annamalai, H., H. Okajima, and M. Watanabe (2007): Possible Impact of the Indian Ocean SST on the Northern Hemisphere Circulation during El Niño. *J. Climate*, **20**, 3164-3189.

Fletcher, C. G., and C. Cassou (2015): The dynamical influence of separate teleconnections from the Pacific and Indian Oceans on the Northern Annular Mode. *J. Climate*, **24**, 778-794., doi:10.1175/JCLI-D-14-00839.1

Johnson, S. J., and Co-authors (2019): SEAS5: The new ECMWF seasonal forecast system. *Geosci. Model Dev.*, **12**, 1087-1117, doi:10.5194/gmd-12-1087-2019

Lee, R. W., S.J. Woolnough, A. J. Charlton-Perez, and F. Vitart (2019). ENSO modulation of MJO teleconnections to the North Atlantic and Europe. *Geoph. Res. Letters*, **46**, 13535–13545. doi:10.1029/2019GL084683

Molteni, F. and F. Kucharski (2019): A heuristic dynamical model of the North Atlantic Oscillation with a Lorenz-type chaotic attractor. *Climate Dyn.,* **52**, 6173-6193, doi:10.1007/s00382-018-4509-4

Molteni, F., T. N. Stockdale, and F. Vitart (2015): understanding and modelling extratropical teleconnections with the Indo-Pacific region during the northern winter. *Climate Dyn.*, **45**, 3119-3140, doi: 10.1007/s00382-015-2528-y.

Tseng, K-C., E. Maloney and E. A. Barnes (2020): The consistency of MJO teleconnection patterns on interannual time scales. *J. Climate*, **33**, 3471-3486, doi:10.1175/JCLI-D-19-0510.1

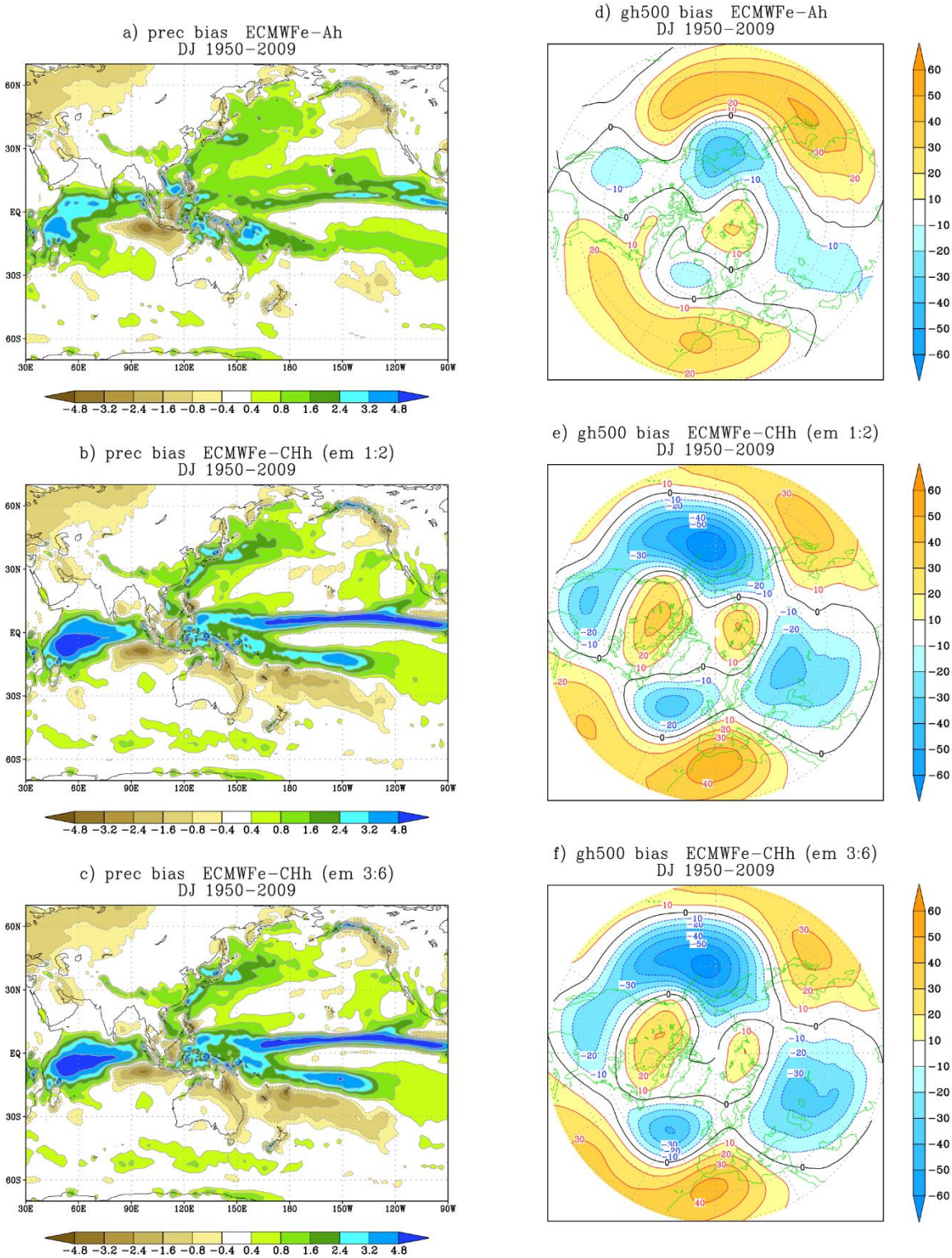

Fig. S3. Rainfall bias over the Indo-Pacific region in DJ 1950-2009 for: (a) the six members of the AMIP-H ensemble, (b) the first two members of the CHist-H ensemble, (c) the last four members of the CHist-H ensemble. (d) to (f): as (a) to (c), for biases in 500-hPa height.

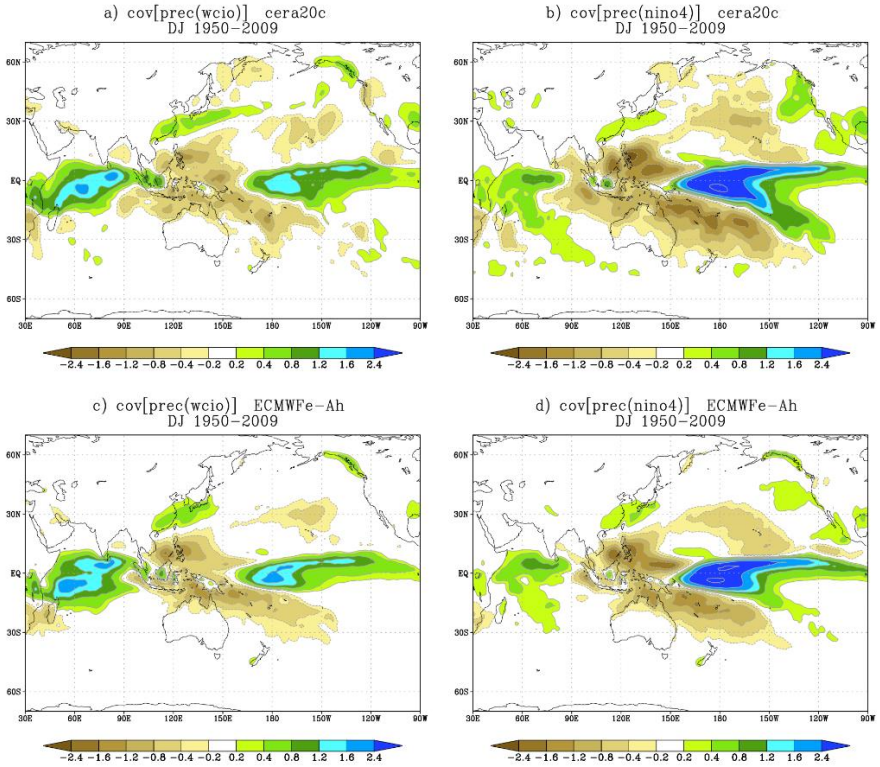

Fig. S4 Covariance of rainfall in the Indo-Pacific domain with normalised indices of rainfall anomalies in the WCIO (a) and NINO4 (b) regions (see Fig. 1 in main paper), from CERA20C data in DJ 1950-2009. (c) and (d): as in (a) and (b) respectively, but from the six members of the ECMWF AMIP-H ensemble.

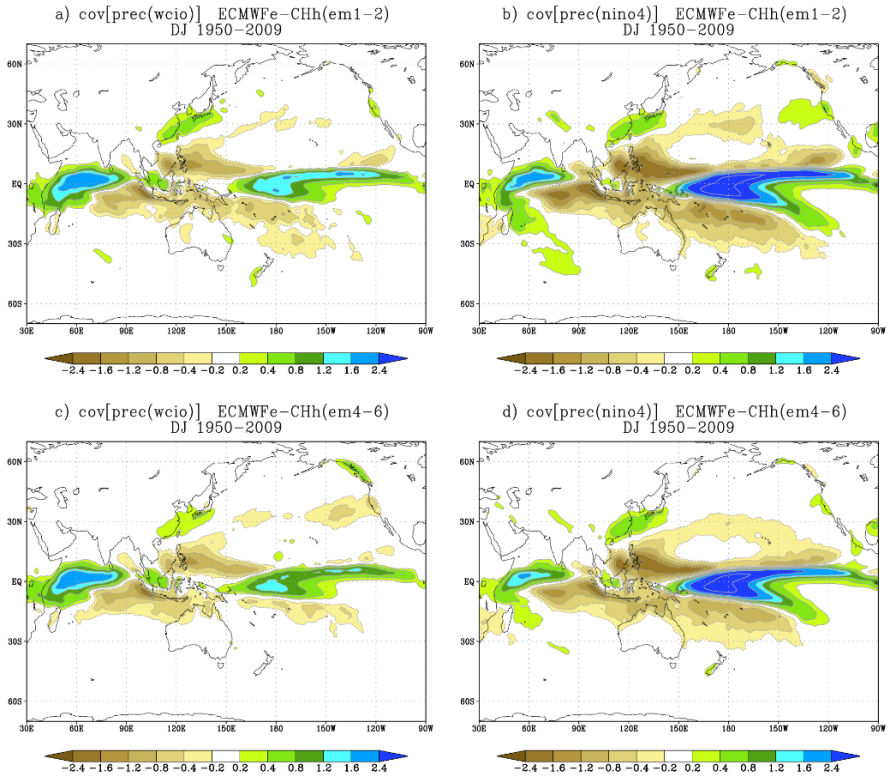

Fig. S5 (a) and (b): as in Fig. S4a and S4b, but for the first two members of the ECMWF CHist-H ensemble; (c) and (d): as (a) and (b), but for the last four members of the CHist-H ensemble.

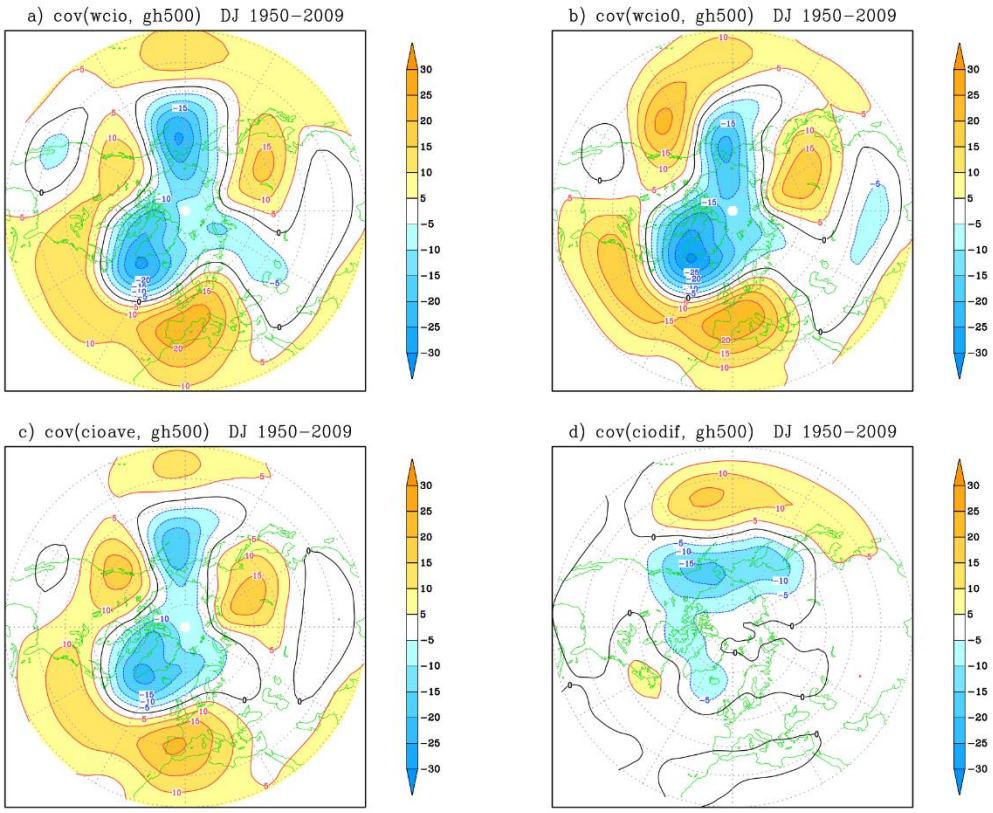

Fig. S6 Covariance of N.Hem. 500-hPa height with normalised indices of rainfall anomalies, from CERA20C data in DJ 1950-2009. (a) for WCIO index (40E-90E, 10N-10S); (b) for WCIO index, after removing the anomaly correlated with NINO3.4 SST; (c) for CIO-ave index (70E-90E, 10N-10S); (d) for CIO-dif index (70E-90E, 10N-0 minus 0-10S).

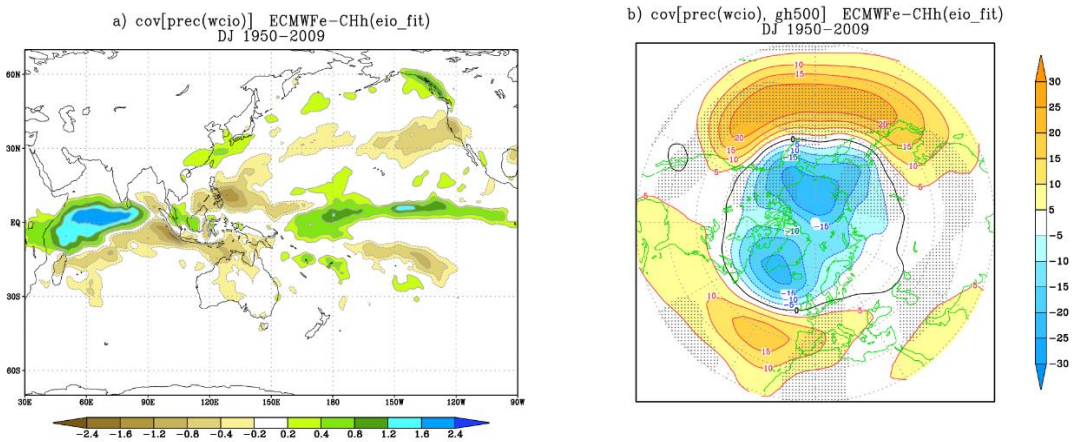

Fig. S7 (a) Covariance of DJ rainfall in the Indo-Pacific domain with the normalised index of WCIO rainfall anomalies, from a CHist-H "merged member" including data from the single ensemble member with best fit between simulated and observed SST anomaly in EEIO during ON; (b) as in (a), but for the WCIO covariance with N.Hem. 500-hPa height in DJ. Stippling indicates areas where differences from the CERA20C pattern in Fig. S6a are significant at a 90% confidence level.